Time-and-spatial-multiplexing tree topology for fiber-optic Bragg-grating sensors with interferometric wavelength-shift detection

A. B. Lobo Ribeiro, Y. J. Rao, L. Zhang, I. Bennion, and D. A. Jackson

A combined time-and-spatial-division-multiplexed tree topology with eight fiber-optic Bragg-grating sensors operating at the 830-nm wavelength was constructed and tested for both quasistatic and periodic strain and temperature measurements. The system uses a interferometric wavelength-shift discriminator and incorporates a reference channel for thermal drift compensation in the output. Dynamic sensor sensitivity, as determined by primary noise sources, is evaluated, and numerical results are presented and compared with experimental results.

Key words: Fiber-sensor multiplexing, fiber Bragg gratings, strain sensors.

1. Introduction

Fiber-optic-based sensors are currently subject to intensive research and development as they potentially offer many advantages compared with those of conventional electronic sensors. Of these new developments, the fiber-optic Bragg-grating (FBG) sensors, which can be written at any arbitrary location along a fiber without increasing the fiber cross section,[1] offers many sensing opportunities in areas such as structural monitoring or medical diagnostics. In this type of application, it is likely that a large number of sensors will be deployed; hence there is a need to develop effective multiplexing topologies.[2,3] In this paper we introduce such a topology that incorporates both spatial and temporal division. To date, most multiplexing topologies for FBG sensors have been based on serial arrays[4]; although this form of multiplexing can be efficient there are problems in that the central reflecting wavelengths of the FBG sensor must all be different by at least 2–3 times the anticipated wavelength range of the sensor. This requirement tends to make the cost of producing the sensors expensive. Further problems with such arrays can be anticipated in practical applications in which the sensing fiber is incorporated into a structure such that it cannot be removed: a single breakage in the fiber at the interface between the electronics and the structure could then make the sensor network inoperative. Another advantage of the topology presented here is that there are no restrictions placed on the central reflecting wavelengths of the FBG sensors [except that they must be within the linewidth (LW) of the illuminating source].

When a simple spatial-multiplexing topology[5] is adopted, the above problems are eliminated. We have developed a fiber-optic reflective tree topology based around a commercially fabricated directional coupler network consisting of seven couplers, indicated in Fig. 1, where 2 FBG sensors are deployed at each output port, giving a total of 8 sensors. These signals are separated by incorporating time-division multiplexing (TDM) into the network. The signal processing is based on an unbalanced interferometer used as a wavelength discriminator[6] (WD) illuminated with a broadband source. The output of the interferometer consists of channeled spectra, essentially m separate sources. When the optical path difference (OPD) of the interferometer is linearly scanned by $\approx 2\pi$ rad, then there are effectively m tunable sources with a tuning range of LW/FSR, where LW is the source LW and FSR is the free spectral range of the interferometer. This multi-

A. B. Lobo Ribeiro is with Grupo de Optoelectrónica, Instituto de Engenharìa de Sìstemans e Computadores, R. José Falcão 110, 4000 Porto, Portugal; Y. J. Rao and D. A. Jackson are with the Physics Laboratory, Applied Optics Group, University of Kent, Canterbury, Kent CT2 7NR, U.K.; L. Zhang and I. Bennion are with the Department of Electronic Engineering, Photonics Research Centre, Aston University, Birmingham B4 7ET, U.K.

Received 18 July 1995; revised manuscript received 18 October 1995.

0003-6935/96/132267-07$10.00/0

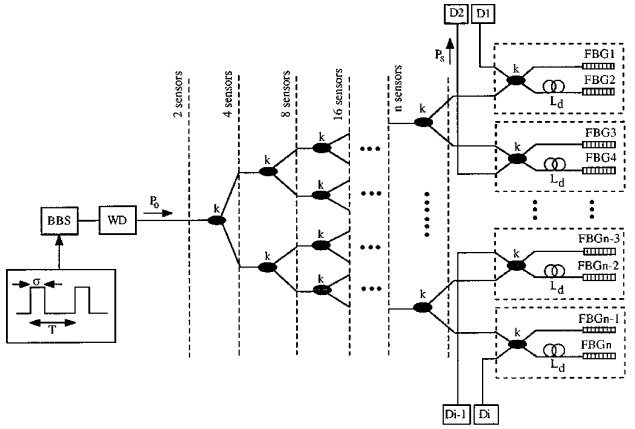

Fig. 1. Multiplexing topology: BBS, broadband source; WD, wavelength discriminator; k's, coupling ratios of the directional couplers; L_d's, delay fibers; FBG1–FBGn, FBG sensors; D1–Di, detectors $(i = n/2)$.

wavelength-tunable source allows pseudoheterodyne signal processing techniques[7] to be used. The FBG sensor reflects a narrow frequency band; thus when the phase of the reflected FBG sensor signal is compared with the scanning signal applied to the interferometer, the reflecting wavelength of the FBG sensor can be accurately measured without ambiguity, provided the measurand-induced wavelength change is less than the FSR. Another advantage of the network presented here is that the mean wavelengths of all the FBG sensors can be identical, which makes for a low-cost network with easy replacement of the FBG sensors in the event of a breakage.

2. Theory

The method used to detect the wavelength shift of the FBG sensor is based on the use of an unbalanced interferometer that behaves as a WD.[6] This interferometer converts the wavelength shift of the light reflected from a strained FBG sensor into an optical phase shift. The induced change in the reflected Bragg wavelength $\Delta\lambda_g$, which is due to the strain perturbation, is proportional to a phase shift $\Delta\phi_g$ through the following relation:

$$\Delta\phi_g = \frac{2\pi(\mathrm{OPD})}{{\lambda_g}^2}\,\Delta\lambda_g = \frac{2\pi(\mathrm{OPD})}{\lambda_g}\,\zeta\Delta\epsilon, \tag{1}$$

where $\Delta\epsilon$ is the change in strain, λ_g is the Bragg wavelength of the FBG sensor, OPD is the optical path difference of the interferometer, and ζ is the normalized strain-to-wavelength-shift responsivity of the grating (a reported value[1,4] of 0.74×10^{-6} $\mu\epsilon^{-1}$). The information contained in the phase-modulated output can be then extracted by the use of the pseudoheterodyne demodulation technique.[7]

A. Multiplexing Topology

The multiplexing topology, shown in Fig. 1, is a tree array of reflective FBG sensors addressed in time and space. This topology is not as efficient as a standard tree coupler array, as more than one photodetector is used; however, it does yield a much better signal-to-noise ratio (SNR) for each sensor for little extra cost, as the returning optical signals suffer significantly less loss. Each pair of sensors (1 and 2, 3 and 4, etc.) is separated spatially by its own fiber output channel, and in each channel both sensors are separated in time through the delay fiber (L_d). To ensure time division in each channel, the following condition must be satisfied:

$$\begin{cases} \dfrac{2nL_d}{c} \geq \sigma \\ T \geq 2\sigma \end{cases}, \tag{2}$$

where n is the refractive index of the fiber guided mode, c is the speed of light, L is the length of the fiber delay lines, and T and σ are the period and the pulse width of the modulation applied to the broadband source, respectively. If the equalities are considered in relation (2) and if P_{peak} is the peak power injected into the input fiber, then the injected average power P_0 is

$$P_0 = (\sigma/T)P_{\mathrm{peak}}. \tag{3}$$

To achieve the desirable condition, i.e., that all the sensors have identical sensitivity, it is necessary to ensure that the average power returned from each sensor is the same. Assuming that there are N sensors in the tree network (Fig. 1), then $(N - 1)$ directional fiber couplers (DC's) and $N/2$ fiber delays are required. The crucial criterion for system design is to ensure that each sensor returns the same average optical power (P_s); it is straightforward to show that, for this condition, all DC's must have the same coupling ratio (k) equal to $1/2$, where k and $(1 - k)$ are the fractional coupled and the transmitted powers, respectively.

The analysis is simplified if it is assumed that losses in fibers, splices, couplers, etc. are lumped together in the couplers, giving a total power attenuation factor of $1 - \gamma$ each time the light crosses a DC. Also we introduce a power attenuation factor $1 - \beta$, which is approximately equal to the total loss in a delay length L_d of fiber and in one splice. $1 - \gamma$ is the lumped loss relative to one DC and one splice. When the above criteria are used, the return power per sensor will be

$$P_s = \left(\frac{\pi}{4\ln 2}\right)^{1/2} R P_0\,\frac{\Delta\lambda_g}{\Delta\lambda_s}\left(\frac{\gamma}{2}\right)^{1+\log_2 N} \tag{4}$$

where R is the FBG maximum reflectivity, P_0 is the average power incident upon the FBG sensor, and $\Delta\lambda_s$ and $\Delta\lambda_g$ are the bandwidths (FWHM) of the source and the FBG sensor, respectively. In Eq. (4) it is assumed that the spectrum of the source is flat over the working range of the FBG sensor. It should be pointed out that it is not possible to get the

same returned optical power for both pulses in each spatial output, because of the loss that is due to the delay fiber in one of the lines and because the coupling ratio of the DC is $1/2$; however it is possible to have identical returned optical power for each spatial channel. Figure 2 shows the returned optical power per sensor, normalized by the input power, as a function of the number of sensors for a lossless system (i.e., $\gamma = 1$) and for operation at the 830-nm wavelength, with a fiber loss of 2.5 dB/km, a coupler loss of 0.2 dB, and a splice loss of 0.1 dB; we have $\gamma = 0.93$ and $\beta = 0.96$ ($L_d = 40$ m).

B. Sensor Sensitivity

In this section, the minimum detectable phase signal $\phi_{\min}$ for the sensors in the system is evaluated, considering the primary noise sources (namely, phase noise, shot noise, and electronic noise). With an analysis similar to that of Ref. 8, and for a SNR of 1, the minimum detectable phase for all three noise sources considered is

$$\phi_{\text{phase}} = \left\{\frac{B\tau_c \exp(-2z)}{4V^2} \times [\cosh(2z) + \sinh(2z) - 2z - 1]\right\}^{1/2}, \quad (5)$$

$$\phi_{\text{shot}} = \left(\frac{8BM^x h\nu_0}{\eta V^2 P_s}\right)^{1/2}, \quad (6)$$

$$\phi_{\text{electronic}} = \frac{h\nu_0}{\eta e_0 VMP_s} \times \left[2B\left(2e_0 i_{\text{dark}} M^{2+x} + \frac{4k_B T}{R_f} + {i_{\text{amp}}}^2\right)\right]^{1/2}, \quad (7)$$

where $z = \tau/\tau_c$ and $\tau = \text{OPD}/c$, τ_c is the coherence time (in our case is defined by the LW of the FBG sensor), B is the system bandwidth, M is the detector multiplication gain, V is the fringe visibility, x is the excess noise index of the photodetector [$0 < x < 1$ for an avalanche photodiode (APD)], η is the photodetector quantum efficiency, h is Planck's constant, ν_0 is the optical frequency of the source, k_B is Boltzmann's constant, T is the absolute temperature, e_0 is the electron charge, i_{dark} is the photodetector dark current, i_{amp} is the noise-current spectral density of the transimpedance amplifier, and R_f is the feedback resistance. Thus, assuming uncorrelated noise sources, the minimum detectable phase signal is

$$\phi_{\min} = \phi_{\text{phase}}^2 + \phi_{\text{shot}}^2 + \phi_{\text{electronic}}^2. \quad (8)$$

Using the above equations together with approximate experimental parameters, we may estimate the SNR as a function of the number of sensors for this topology. The parameters used were $\Delta\lambda_g = 0.2$ nm, $\lambda_g = \lambda_s = 830$ nm, $\Delta\lambda_s = 20$ nm, $P_{\text{peak}} = 1$ mW ($P_0 = 250$ μW for 50% duty cycle plus 50% that is due to the interferometer and assuming no losses), $R = 0.9$, OPD = 700 μm, $V = 0.86$, $B = 1$ Hz, $T = 300$ K, $R_f = 10$ kΩ, $i_n = 2.7$ pA/$\sqrt{\text{Hz}}$ (for Hamamatsu C5460 detector). For operation at 830 nm, $\eta(\text{Si}) = 0.74$, $x(\text{Si}) = 0.3$, and $i_{\text{dark}}(\text{Si}) = 1$ nA. Figure 3 shows the variation in sensor sensitivity in terms of minimum detectable strain as a function of N for all the noise sources considered. The minimum variation in strain is related by the minimum detectable phase change through relation (1). Together with these primary noise sources, other sources of noise exist that will further degrade the performance of the sensing network. The most relevant are those associated with (a) the $1/f$ noise of the receiving electronics, (b) the polarization effects on the interferometer that will reduce the fringe visibility, and (c) the mechanical stability of the interferometer and subsequent $1/f$ acoustic noise. Their relative importance must be assessed for each individual real case.

3. Experiment

Figure 4 schematically shows the experimental arrangement. The multiplexing topology is identical to that shown in Fig. 1 for $N = 8$ and was performed by an 1×8 fiber-optic splitter especially designed for spatial-multiplexing systems. There are four out-

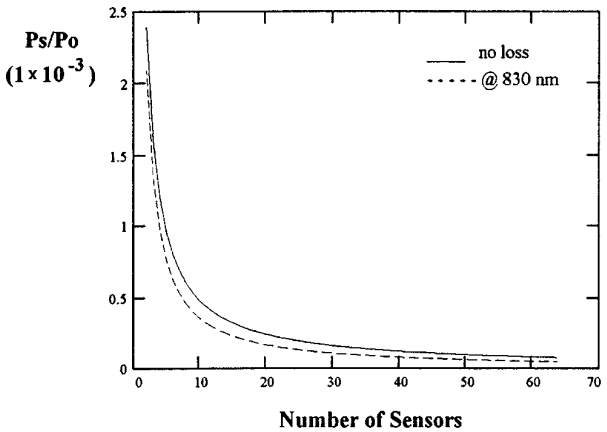

Fig. 2. Returned light power from each sensor, normalized by the average input power.

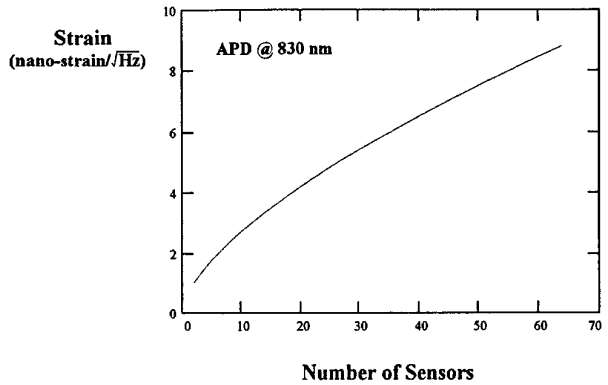

Fig. 3. Total strain sensitivity ($\epsilon_{\min}$) considering all noise sources for operation at 830 nm by the use of an APD detector with optimum multiplication gain.

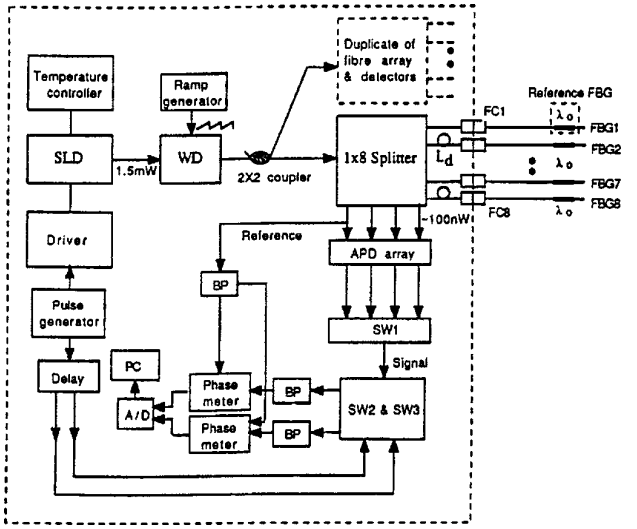

Fig. 4. Schematic diagram of the multiplexing system: SLD, superluminescent diode; FC1 and FC8, fiber connectors; BP's, bandpass filters; SW's, switches; A/D, analog–digital converter.

put ports, and each port contains two fiber transmission lines with a differential delay length of 40 m (fiber attenuation of 2.5 dB/km at 830 nm), corresponding to a time delay of 400 ns. The light source was a pigtailed temperature-stabilized superluminescent diode with a bandwidth of 18.5 nm and a mean wavelength of 830 nm, supplied by Superlum Ltd. (Moscow). It was modulated by a square waveform at a frequency of ≈1.1 MHz with a pulse width of ≈300 ns (duty cycle ≈1/3). The average emitted output power from the single-mode pigtail was greater than 1.5 mW. Eight identical FBG sensors, with nominal Bragg wavelengths of 830 nm (bandwidth ≈ 0.2 nm) and peak reflectivities of 90%, were connected to the eight output ends of the 1×8 splitter by fiber connectors, as shown in Fig. 4. It would be feasible to interrogate a further eight FBG sensors by duplicating part of the network (using the second output port of the 2×2 coupler in Fig. 4) without any reduction in the SNR of each sensor. This coupler was used in the system in order that the returned power to the detectors would be the same as if the network contained 16 rather than 8 FBG sensors. The WD used in this work was a bulk Michelson interferometer (Queensgate Instruments Ltd.) with an OPD of 702 μm (equal to a FSR of 0.98 nm). The piezoelectric transducer (PZT) in the WD was driven by a ramp (serrodyne) modulation function at a frequency ω_c of 300 Hz in order to recover the interference signal by the pseudoheterodyne technique.[7] The return pulse signals from the FBG sensors were detected by an array of four APD's with transimpedance amplifiers, giving a combined variable gain of between 0.2 and 10 V/μW and a bandwidth of 10 MHz (noise-equivalent power 0.2 $\mathrm{pW}/\sqrt{\mathrm{Hz}}$). The signals from the APD array were selected by the use of a switch (SW1). Thus each APD receives the returned signals from two FBG sensors separated in time by ≈400 ns, and then they are demultiplexed by two high-speed switches (SW2 and SW3) controlled by the delayed electric pulses produced by the pulse generator, as shown in Fig. 4. After bandpass filtering at the fundamental frequency (ω_c) of the serrodyne signal, the sinusoidal output that corresponds to each sensing FBG was sent to a phase meter (lock-in amplifier) to determine the phase change relative to the reference FBG sensor (see Fig. 4). This reference FBG sensor was deployed strain free and located in the same temperature environment as the sensing FBG. The output phase signal from the lock-in amplifier was sent to a PC through a 12-bit analog-to-digital converter. The resolution of the phase meter was 0.1°, which corresponds to a wavelength resolution of ≈0.27 pm for the FSR of 0.98 nm determined by the OPD of the WD.

4. Results and Discussion

The detected output signals from the APD array that correspond to the eight FBG sensors are shown in Fig. 5(a). In order to show all the pulses clearly, we adjusted the amplitudes of these pulses by changing the joint loss within the fiber connectors. Figure 5(b) shows signals from FBG1 and FBG2 before and after gating. For visualizing interference effects at the output pulses, the WD was modulated by the application of a serrodyne signal to the PZT in one of the arms of the interferometer. The glitches observed in the demultiplexed pulses result from high-frequency electronic reflections in the circuit board because of mismatched impedances. The demultiplexed signals that correspond to four FBG sensors when the WD is modulated over one fringe are shown in Fig. 5(c). To investigate the sensitivity of the system to low-frequency strain perturbations and the cross talk between two adjacent TDM channels (FBG3 and FBG4), we applied a 3.43-με rms strain variation to FBG3 at a frequency of ≈12 Hz. Figures 6(a) and 6(b) show the power spectra of the phase difference output (i.e., difference between the sensor and the reference FBG's) that correspond to the two channels, respectively. The SNR of the component at 12 Hz [Fig. 6(a)] of 31 dB normalized to 1-Hz bandwidth corresponds to a minimum detectable strain perturbation of $\approx 230\ \mathrm{n}\epsilon/\sqrt{\mathrm{Hz}}$. Figure 6(b) (FBG4) shows that the cross-talk signal is just above the noise floor from which a cross-talk level of ≈−30 dBV is estimated (a similar result was obtained when the strain signal was applied to FBG4). Identical strain sensitivity was obtained with the same amplitude signal applied at 1-Hz frequency.

To obtain the strain-to-phase shift responsivity ($\Delta\phi/\Delta\epsilon$), a sensing FBG was mounted between a fixed block and a precision translation stage, separated by a distance of ≈40 cm. The experimental result is shown in Fig. 7(a), and from this we obtained 0.237°/με, which corresponds to a strain-to-wavelength ($\Delta\lambda_g/\Delta\epsilon$) coefficient of ≈0.64 pm/με. For the thermal-drift-compensated measurement, a quasi-static strain was applied to the FBG, which was glued to a PZT. We applied several ≈0.26-Hz strain

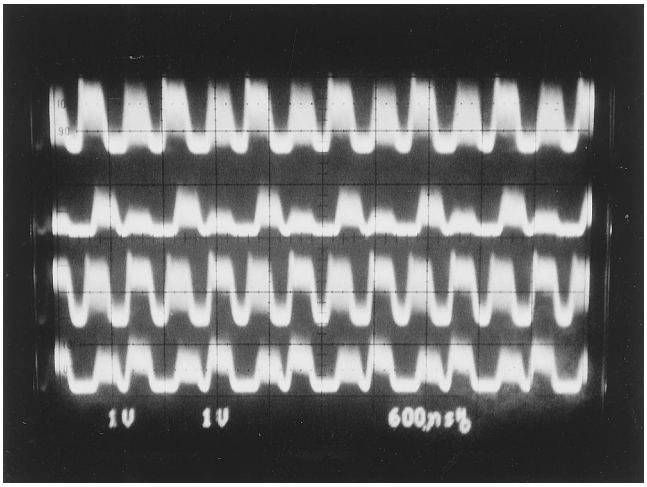

(a)

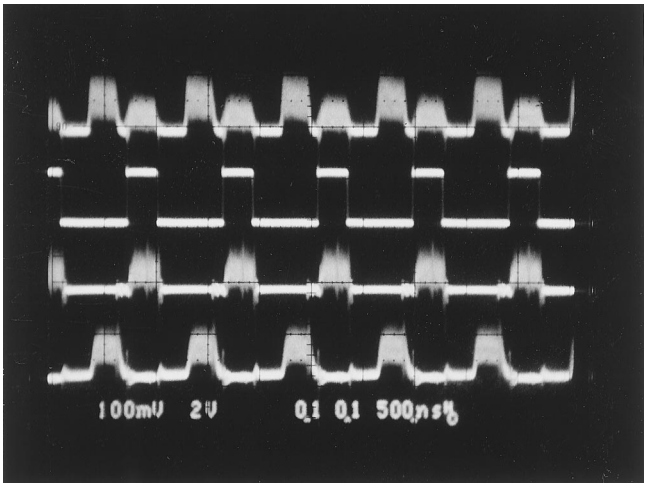

(b)

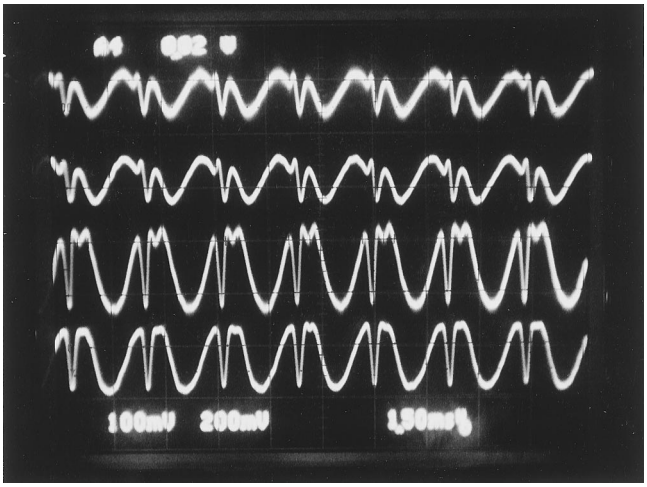

(c)

Fig. 5. (a) Photodetected return pulse signals from eight FBG sensors. Each trace corresponds to the detected signals from each output port of the splitter. (b) TDM–demultiplexing pulses from FBG1 and FBG2 before and after gating (the gating signal is the second from the top of the figure). (c) Demultiplexed signals (after filtering) from four FBG sensors.

steps of ≈9-με peak-to-peak amplitude, and it can be seen from the experimental results shown in Fig. 8(a) that a strain resolution of 1.2 με (determined by the noise level) was achieved with a 30-Hz measurement bandwidth. The overall strain range shown in Fig. 7(a) was ≈1.5 mε; hence the achieved range-to-resolution ratio was 1250:1. One sensing FBG was placed in an oven to obtain the temperature-to-phase shift responsivity ($\Delta\phi/\Delta T$). The experimental measured value was 2.49°/°C, as shown in Fig. 7(b).

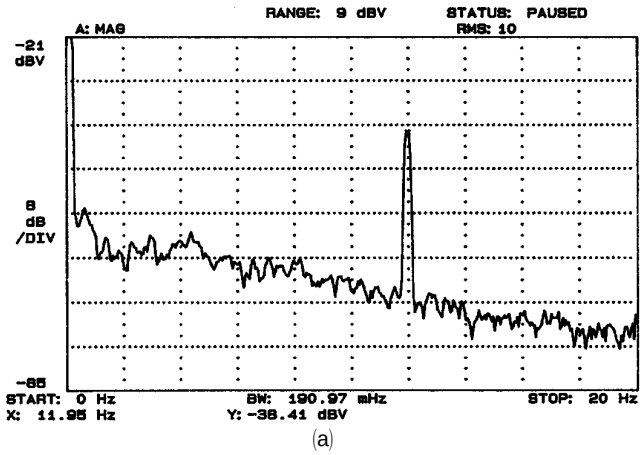

(a)

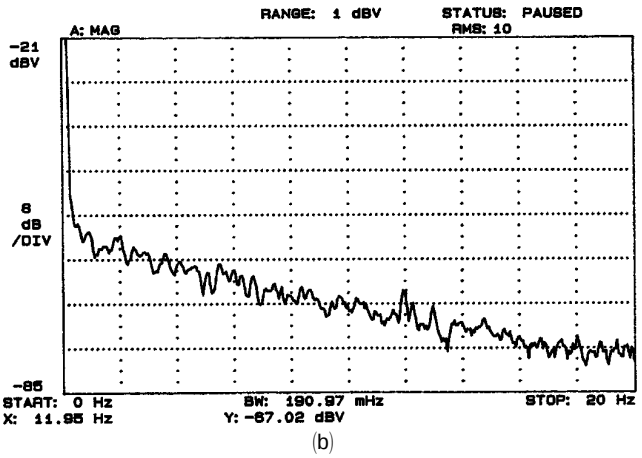

(b)

Fig. 6. (a) FBG3 demodulated output signal when a strain variation of 3.43-με rms (frequency ≈12 Hz) is applied. (b) Output signal from FBG4 of the same TDM channel when a strain variation of 3.43-με rms (frequency ≈12 Hz) is applied to FBG3; note the very low level of cross talk.

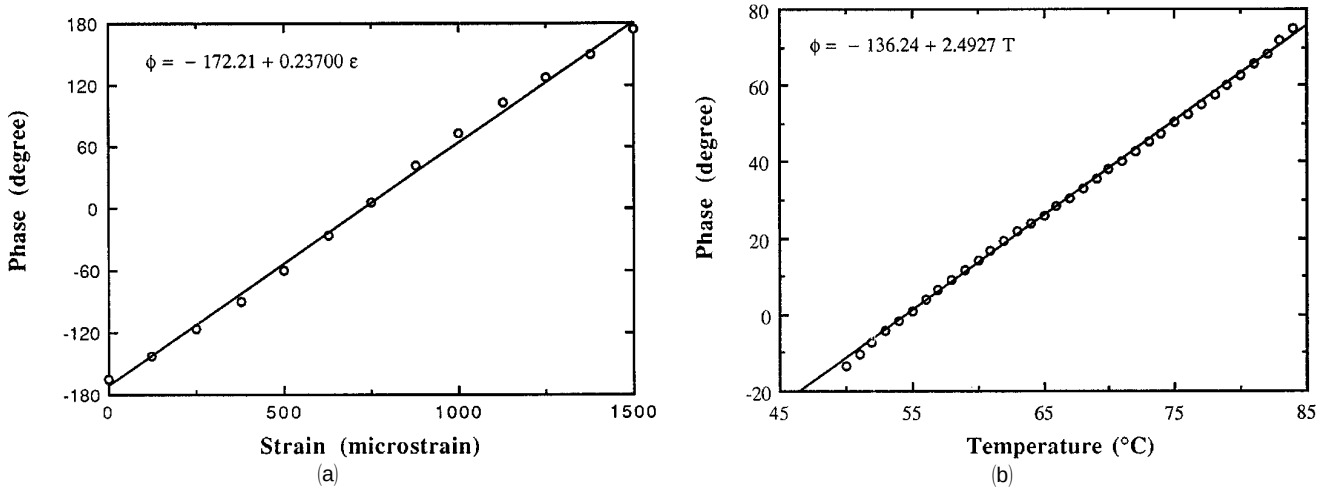

Fig. 7. Experimental results of (a) strain, (b) temperature measurements.

This corresponds to a temperature-to-wavelength $(\Delta\lambda_g/\Delta T)$ coefficient of 6.79 pm/°C. Figure 8(b) shows the quasi-static temperature resolution when the FBG was heated periodically, with ≈0.13-Hz temperature steps of ≈1.4 °C peak-to-peak amplitude; from this figure the temperature resolution is ≈0.12 °C. The overall temperature range shown in Fig. 7(b) was ≈35 °C; hence the range-to-resolution ratio achieved was 292:1, however, the overall absolute temperature range that corresponds to a 2π phase change in the WD is 137 °C, which gives a noise limitation range-to-resolution ratio of 1142:1.

From the discussion in Section 2, the sensitivities imposed by the primary noise sources (with experimental measured values of $P_s = 33.3$ nW with 1/3 duty cycle, $V = 0.64$, $N = 8$, and an APD gain of 200) are $\phi_{\text{phase}} = 0.62\ \mu\text{rad}/\sqrt{\text{Hz}}$, $\phi_{\text{shot}} = 30.52\ \mu\text{rad}/\sqrt{\text{Hz}}$, and $\phi_{\text{electronic}} = 5.70\ \mu\text{rad}/\sqrt{\text{Hz}}$, which are equivalent to an overall phase sensitivity of $\phi_{\text{min}} = 31.1\ \mu\text{rad}/\sqrt{\text{Hz}}$. This corresponds to an overall strain sensitivity of $\epsilon_{\text{min}} = 7.5\ \text{n}\epsilon/\sqrt{\text{Hz}}$ [from the experimental results of Fig. 7(a): 4.14 μrad/nε]. In addition to the primary noise sources, we must also include the $1/f$ noise (frequencies <100 Hz) of the electronic detection system, which includes the gating process; this was found to increase the noise floor by a factor of 28.2 (≈29 dB), which is close to the experimental value of 230 $\text{n}\epsilon/\sqrt{\text{Hz}}$. As expected, these values were found to be dominated by the $1/f$ noise, which is not possible to model theoretically. The analysis presented in Subsection 2.B. is for sensors operating outside the $1/f$ noise region. For sensors operating in this region, such as structural strain sensors, the

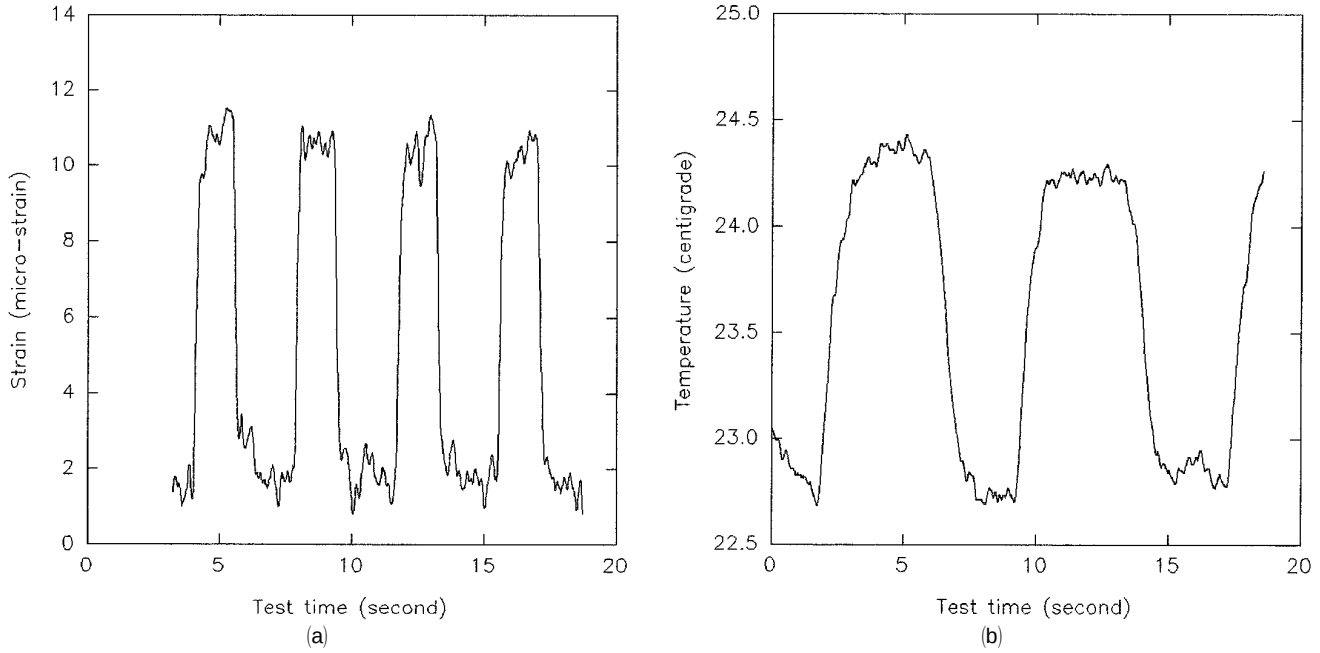

Fig. 8. Responses to quasi-static perturbations: (a) 0.26-Hz strain perturbation, (b) 0.13-Hz temperature perturbation.

noise floor is usually determined by the $1/f$ noise of the receiving electronics; hence in this regime it is advantageous to use an APD with large gain. The upper limit of the gain is determined by the requirement that the level of optical noise must not exceed the $1/f$ noise floor of the electronics. The network was tested for eight FBG sensors, but, in principle, it can be extended to support 16 FBG sensors without affecting the SNR of any sensor. In addition, the interchangeability of this system was demonstrated when the FBG sensors were moved among the different output ports, and virtually no change in sensor performance occurred in this procedure. Comparing this topology with a series topology,[4] we find that the advantages are (1) the operational wavelength range of each sensor can be identical and is unaffected by the number of sensors to be multiplexed, hence minimizing the cost of fabricating the FBG sensors; (2) flexibility in deployment as there is one FBG per fiber; (3) easy sensor maintenance in the event of damage; (4) no intrinsic cross talk. The disadvantage of this multiplexing topology is that more optical fiber is required together with further $(N/2 - 1)$ detectors compared with the most efficient implementation of a fiber tree topology, which could be operated with a single detector.

5. Conclusion

A combined spatial-and-TDM topology with interferometric wavelength-shift detection by the use of FBG sensors has been investigated. Numerical results of sensor sensitivity were obtained for operation at a wavelength of 830 nm by an APD. The concept was demonstrated with eight FBG sensors and applied to the measurement of periodic and slowly varying parameters, but could support 16 FBG sensors without any detriment in performance of the individual sensors. A range-to-resolution ratio of 1250:1 for quasistatic strain and 292:1 for temperature have been achieved with a measurement bandwidth of 30 Hz.

This study was partially supported by the Welcome Trust Foundation and Engineering and Physical Sciences Research Council. A. B. Lobo Ribeiro gratefully acknowledges the help received from J. L. Santos and the financial support from Programa PRAXIS XXI.

References

1. G. Meltz, W. W. Morey, and W. H. Glenn, "Formation of Bragg gratings in optical fiber by a transverse holographic method," Opt. Lett. **14,** 823–825 (1989).
2. D. A. Jackson, "Selected multiplexing schemes for fibre optic interferometric sensors," in *Distributed and Multiplexed Fiber Optic Sensors III,* A. D. Kersey and J. P. Dakin, eds., Proc. SPIE **2071,** 68 (1993).
3. W. W. Morey, J. Dunphy, and G. Meltz, "Multiplexing fiber Bragg grating sensors," in *Distributed and Multiplexed Fiber Optic Sensors,* A. D. Kersey and J. P. Dakin, eds., Proc. SPIE **1586,** 216 (1993).
4. R. S. Weis, A. D. Kersey, and T. A. Berkoff, "A four-element fiber grating sensor array with phase-sensitive detection," IEEE Photon. Technol. Lett. **6,** 1469–1472 (1994).
5. A. B. Lobo Ribeiro, Y. J. Rao, and D. A. Jackson, "Multiplexing interrogation of interferometric sensors using dual multimode laser diode sources and coherence reading," Opt. Commun. **109,** 400–404 (1994).
6. A. D. Kersey, T. A. Berkoff, and W. W. Morey, "High-resolution fibre-grating based strain sensor with interferometric wavelength-shift detection," Electron. Lett. **28,** 236–238 (1992).
7. D. A. Jackson, A. D. Kersey, and M. Corke, "Pseudo-heterodyne detection scheme for optical interferometers," Electron. Lett. **18,** 1081–1082 (1982).
8. J. L. Santos and D. A. Jackson, "Coherence sensing of time-addressed optical-fiber sensors illuminated by a multimode laser diode," Appl. Opt. **30,** 5068–5076 (1991).